Replication of Emergent Foraging Strategies under Resource Competition in Multi-Agent Systems

GONÇALO RODRIGUES, 90256, LEONOR CARVALHO, 99623, and DINIS MATOS, 100146, GROUP 27

1 Introduction

Effective foraging strategies are fundamental to survival and reproduction, shaped by both environmental constraints and competitive pressures [Fiveable 2024]. While the Marginal Value Theorem provides optimal predictions for isolated foragers, it does not fully account for the impact of competition on the evolution of phenotypic traits[Abrams 2000; Charnov 1976]. Yet, empirical evidence suggests that identical ecological niches can support multiple viable strategies[Gould 1989; Levin 1992]. For example, within the same taxonomic class, *Hydra* forage without moving, while limnomedusae actively hunt [Hyman 1940; Rosenberg et al. 2007]. Similarly, sloths and colobus monkeys are both arboreal herbivores but differ in movement patterns and metabolic rates. These findings highlight the evolutionary potential for strategic diversity, even under similar environmental conditions [Nowak 1999; Struhsaker 1997].

Computational models provide powerful tools for understanding the mechanisms underlying such diversity and testing theoretical predictions about evolutionary outcomes under different competitive scenarios. However, the reliability of these insights depends critically on model validation and reproducibility. Replication studies are therefore essential for validating computational models and ensuring reproducibility in evolutionary biology.

Our work addresses these needs through two main objectives. First, we independently reproduce the agent-based model proposed by [Kim et al. 2025], in which movement speed and perceptual acuity evolve under metabolic constraints in a spatially explicit foraging environment. We aim to validate their core finding that competitive pressure favors metabolically efficient over individually optimal strategies, providing quantitative verification of their predictions. Second, we introduce a novel multi-species extension that examines competitive dynamics between populations with different species, a scenario not addressed in the original work that better reflects natural ecological complexity.

2 Methodology

2.1 Reimplementation of the Baseline Model

To replicate the baseline model accurately, it is essential to clearly specify the key components that define the system's dynamics. These components include the state variables of each agent and the environment, the possible actions agents can take, and the observations they can make during simulation.

Agent State:

- **Position:** $(x_i, y_i) \in [0, L]^2$ (2D periodic space)
- **Energy Level:** $E_i \in \mathbb{R}^+$ current metabolic energy
- **Phenotypic Traits:** $\phi_i = (s_i, a_i)$ where s_i is movement speed and a_i is perceptual acuity
- **Movement Phase:** Run/Tumble or Ballistic indicator
- **Orientation:** $\theta_i \in [0, 2\pi]$

Environment State:

- **Resource Distribution:** $R = \{(x_r, y_r)\}$ (active resource locations)
- **Population Composition:** complete agent state set
- **Time:** t (simulation time step)

Actions

- **Run Phase:** maintain heading θ_i at speed s_i
- **Tumble Phase:** randomly reorient with new angle $\theta_i \sim \text{Uniform}[0, 2\pi]$
- **Ballistic Movement:** toward nearest visible resource

Observations

- **Set of detected resources**: $\{r_j : \|r_j - (x_i, y_i)\| \leq a_i\}$
- **Nearest Resource:** distance and bearing to nearest resource
- **Internal energy level:** current energy level E_i
- **Movement Timer:** time since last tumble

Using this foundation, we reproduced the original experiments to evaluate the emergence of multiple foraging strategies under different resource density and competition levels, using the same metrics as the original study.

We implemented a 2D square domain with periodic boundary conditions where food resources appear randomly over time according to a Poisson process with rate λ. Agents move continuously across the environment and expend energy based on their phenotypic traits. Key parameters such as grid size, agent count, resource regeneration delay, and energy values were matched to those reported in the original paper.

Each agent is defined by two traits: speed (s) and perceptual acuity (a). These influence both movement cost and foraging success. Agents use a simple reactive strategy—moving toward nearby resources when detected, or otherwise exploring randomly. The energy cost per time increases with speed and acuity, following Eq. (1).

$$C(s, a) = c_s \times s^2 + c_a \times a \tag{1}$$

where c_s and c_a are fixed coefficients representing the metabolic cost of movement and perception, respectively.

At each time step, agents may reproduce and/or die based on their net energy gain (Eq. 2):

$$\epsilon(s, a \mid r) = \nu(s, a \mid r) \times F - C(s, a) \tag{2}$$

where $\nu(s, a \mid r)$ is the expected number of resources collected per time step, and F is the energy gained per resource. Population dynamics are governed by stochastic processes involving phenotype-dependent birth and death rates, which are functions of $\varepsilon(s, a \mid r)$. These rates determine the likelihood of an agent reproducing or dying at each time step, allowing for adaptive selection over successive generations.

Our implementation closely follows the agent-based model and mean-field approximation described in the original paper. We used

Authors' Contact Information: Gonçalo Rodrigues, 90256; Leonor Carvalho, 99623; Dinis Matos, 100146, GROUP 27.

discrete-time simulations with fixed time steps and implemented trait-based cost functions and reproduction mechanisms as specified.

The mean-field model approximates the population dynamics deterministically by assuming a homogeneous population with phenotype (s, a). Under this assumption, the steady-state population is given by Eq. 3.

$$n^*(s,a) = n^*(\phi) = \frac{\Lambda}{C(\phi) + b(E^*)\ln 2 \cdot E^*} \tag{3}$$

where $\Lambda = \lambda F$ represents the total energy influx to the system as a product of the resource generation rate,λ, and the energetic value per resource, F. The denominator represents the average net energy rate expended by an individual agent, combining metabolic cost $C(\phi)$ with the energy cost of reproduction $b(E^*)\ln 2 \cdot E^*$.

To ensure comparability with the original study, we adopted the same evaluation metrics across all experiments. These include the net energy gain rate $\varepsilon(s, a \mid r)$, steady-state population size n^* for homogeneous populations, the frequency and survival of phenotypes under competitive settings, and the correlation (Eq. 4) between phenotypic traits across generations. These metrics capture both individual-level performance and population-level dynamics, and were used to assess alignment between our reimplementation and the original results.

$$\rho_{s,a} = \frac{\mathrm{Cov}(s,a)}{\sqrt{\mathrm{Var}(s)\,\mathrm{Var}(a)}} \tag{4}$$

All simulations were performed in a square domain of side length $\Omega = 1$, using a time step of $\Delta t = 0.1$. Agents had initial phenotypes uniformly sampled from the range $(s_i, a_i) \in (0, 0.2)^2$, and their movement persistence was described by a persistent length $\eta = 2^{-4}$. The metabolic costs associated with speed and acuity were set to $c_s = 1.6 \times 10^2$ and $c_a = 4$, respectively. Additional parameters included $\alpha = 4$, $K_b = 10$, and $K_d = 1$, which modulated energy dynamics and resource interaction. Offspring were placed near parents with spatial noise drawn from a normal distribution with standard deviation $\sigma_x = \sigma_y = 2.5 \times 10^{-3}$. The remaining parameters specific to each experiment are presented in Table 1.

The main bottleneck of this simulation, is the number of resources present on the environment, since in every step, each agent calculates its distance to every resource on the environment, in order to find out if the closest resource is inside its perception range. To solve this problem, a spatial grid was implement, to reduce the need to search all resources, to only the ones in the surrounding cells, and on top of that, an early-exit circular shell search, to remove redundant resources from the list to calculate distances.

2.2 Extension with Novel Agent Variants

This extension investigates how varying the availability and nutritional value of resources affects species prevalence and phenotype adaptation. Four different species of agents were evaluated in an environment designed to maintain constant overall nutritional availability while varying the characteristics of resource distribution.

For each pair of resource parameters (λ, f), we conducted 10 independent simulations. Each simulation spanned 1,000 time steps. The values of λ and f were chosen to maintain a constant overall nutritional availability, allowing us to isolate the effect of the characteristics of the distribution of the resources on the performance of the agent. During each run, population frequencies and trait distributions were recorded and averaged to assess species dominance and phenotype optimization.

The following parameters were used for all simulations:

- **Initial Agent Count**: 400 agents distributed uniformly across all species
- **Initial Phenotypic Distribution**: speed and acuity were uniformly generated from the following domain $(s, a) \in (0.2, 0.2)^2$
- **Mutation Rate**: [placeholder — e.g., 0.05 per trait per reproduction]

To explore ecological differentiation, we extended the original agent design by introducing three specialized variants that modify baseline behavior through simple, biologically inspired constraints. These new species share the same underlying evolutionary framework and trait system as the original Agent but differ in their decision logic and reproduction strategy:

- **SlothAgent**: A minimal effort variant of the baseline agent that remains stationary unless a resource is within its field of view. In this idle state, the agent's metabolic rate is dependent only on its acuity trait, conserving energy.
- **RaptorAgent**: An aggressive forager that modifies the original agent's movement dynamics by increasing its speed when moving toward visible resources by a factor of 1.5, but doubling the rate of energy expenditure on movement during these bursts.
- **TurtleAgent**: This variant alters the reproductive strategy of the baseline agent by increasing by a factor of 3 the metabolic energy needed for the reproductive rate to be 50%, but producing 3 offspring when it reproduces.

3 Results

This section presents the results of our reimplementation of the agent-based foraging model introduced by [Kim et al. 2025]. We organise our results following the original paper's four-part evaluation structure, with each subsection examining a distinct dimension of agent behaviour and population dynamics: energy efficiency, population equilibrium, strategy competition, and trait diversity. Our goal is to determine whether the same qualitative patterns and quantitative outcomes emerge under similar conditions, providing direct comparisons with the original results to validate consistency and identify any deviations.

3.1 Optimal Foraging of Individual Agent

We begin by analysing the optimal foraging strategy for a single agent. We numerically computed the net energy gain rate $\epsilon(s, a|r)$ for agents with varying speed s and acuity a in environments containing $r \in 100, 200, 300$ resources. Both our reimplemented results and the original findings from [Kim et al. 2025] are presented in Fig. 1.

Fig. 2 illustrates the relationship between acuity and average trajectory length $L(a|r)$ and $\frac{d}{da}\left[g^2(a|r)\right]$, where $g = L^{-1}$. At high acuity, L converges to to the average minimum distance L_0, while

Table 1. Experimental settings and data generation parameters.

Experiment	Population Setup	Key Parameters
Individual Agent Foraging	Single agent in isolation	$N = 1$, $E_0 = 0$, $\beta = \delta = \delta_0 = 0$, $r = 100, 200, 300$, F, steps = 1000
Competition	Homogeneous population	$N = 50, 500$, $(\lambda, F) = (200, 1)$, $\sigma_s = \sigma_a = 0$, $\beta = \delta = 1$, $\delta_0 = 5 \times 10^{-3}$, $\sigma_s = \sigma_a = 0$, steps = 1000
Trait Correlation	Heterogeneous population, no mutation	$N = 10^3$, $(\lambda, F) = (12.5, 16), (100, 2), (400, 0.5)$, $c = 2^{-6}, 2^{-5}, ..., 2^0$, $\sigma_s = \sigma_a = 0$, steps = 2000, simulations = 40
Coexistence Study	Heterogeneous population with mutation	$N = 10^4$, $(\lambda, F) = (50, 4), (200, 1), (800, 0.25)$, $\beta = 0.5$, generations = 50, 100, 400, $\sigma_s = \sigma_a = 3.75 \times 10^{-4}$, simulations = 80

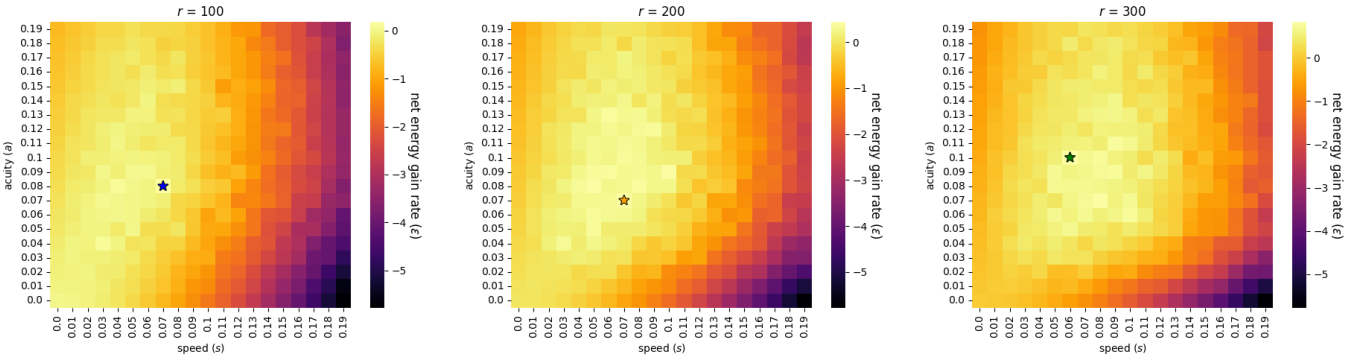

(a) Re-implemented heatmap of $\varepsilon(s, a)$ for $r = 100$. (b) Re-implemented heatmap of $\varepsilon(s, a)$ for $r = 200$. (c) Re-implemented heatmap of $\varepsilon(s, a)$ for $r = 300$.

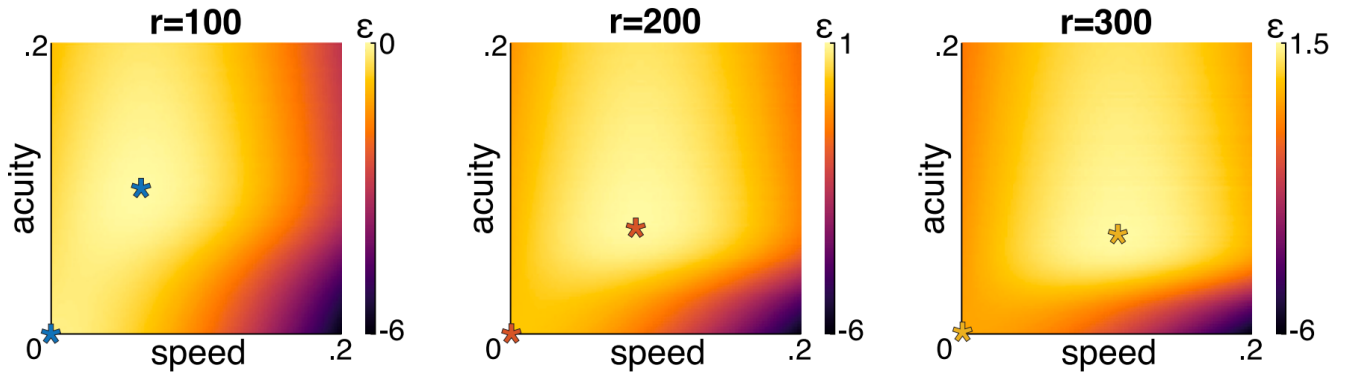

(d) Original heatmaps from [Kim et al. 2025] for $\varepsilon(s, a)$ at $r = 100, 200, 300$.

Fig. 1. **Optimal foraging strategy for a single agent.** Top row: our reimplementation of $\varepsilon(s, a)$ for different resource levels r, with maxima indicated by ★. Bottom: original results from [Kim et al. 2025] with maxima marked by $*$.

at low acuity, trajectory lengths tend to infinity, consistent with the original results.

3.2 Steady-State of a Population Using Single Strategy

Fig. 3 (top) shows the population size $N(\phi)$ over time and the corresponding mean-field predictions for the steady-state size n^*, across different phenotypes. The agent-based simulations converge towards the theoretical predictions for both high and low metabolism strategies. The bottom row reproduces the original results from [Kim et al. 2025], showing similar qualitative behaviour and steady-state values.

3.3 Selection Between Strategies with the Same Metabolic Cost

To investigate whether strategies with the same metabolic cost can coexist under competition, we simulated populations initialized with multiple iso-cost phenotypes. As shown in Fig. 4, the surviving strategy varies depending on the resource environment, with

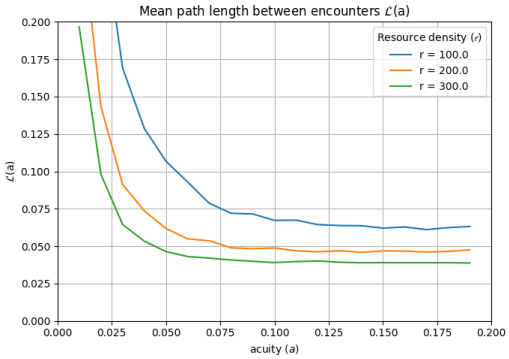

(a) Re-implemented average trajectory length $L(a \mid r)$ for varying acuity.

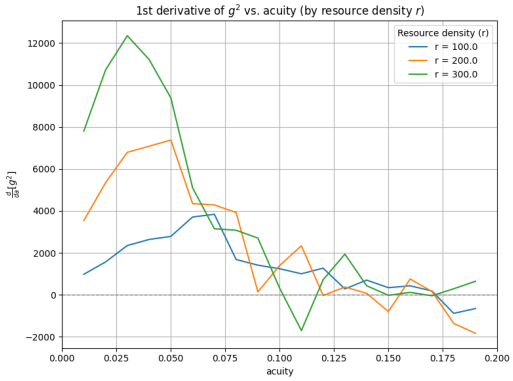

(b) Re-implemented derivative $\frac{d}{da}\left[g^2(a \mid r)\right]$.

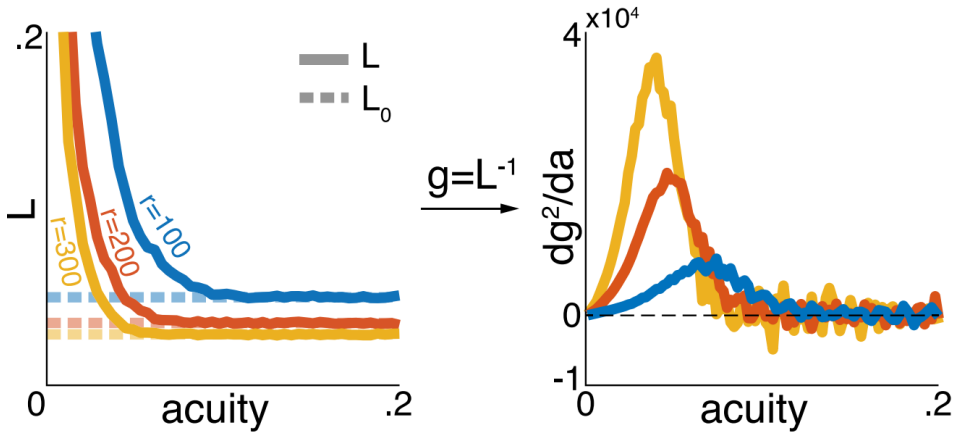

(c) Original results from [Kim et al. 2025] for $L(a \mid r)$ and $\frac{d}{da}\left[g^2(a \mid r)\right]$.

Fig. 2. **Optimal foraging strategy of a single agent.** Top row: our reimplementation of the average trajectory length $L(a \mid r)$ and the acuity derivative $\frac{d}{da}[g^2(a \mid r)]$. Bottom: original results from [Kim et al. 2025].

high-speed and high-acuity phenotypes favored in clustered settings. When compared to the original study, our reimplementation produces similar selection patterns, although with slightly greater dispersion.

3.4 Coexistence of Phenotypic Attributes

We next analysed the equilibrium correlation between speed and acuity across simulations with different resource densities. As shown in the top row of Fig. 5, speed and acuity tend to be positively correlated at equilibrium. This effect is consistent across simulations, as indicated by the mean correlation trend. These results are consistent with the original findings shown in the bottom panel.

We also examined the distribution of phenotypes at equilibrium (Fig. 6). Our reimplementation confirms that resource density influences the shape of the phenotypic distribution. In particular, intermediate-resource environments tend to show greater diversity in phenotypes; however, we do not observe the emergence of clearly separated phenotypic subgroups as in the original results from [Kim et al. 2025], shown in the lower panel of Fig. 6.

3.5 Additional Work: Optimization of species traits in a multi-species ecosystem

As illustrated in Figs. 8 and 9, the raptor agent demonstrates superior performance in moderate and sparse environments, effectively leveraging its speed to access limited resources. In contrast, the basic agent dominates when resources are abundant but less nutritious, due to its energy efficiency. The sloth agent tends to adopt high speed and medium acuity phenotypes in sparse environments and shifts toward lower speeds as resources become more available. The turtle agent shows greater phenotypic variability across conditions, but does not outperform other agents in any scenario.

4 Discussion

Table 2 presents a non-exhaustive list of problems encountered during replication and the assumptions we made to address them.

Our replication efforts reveal partial agreement with the original findings of [Kim et al. 2025]. Our single-agent analysis demonstrates strong qualitative agreement with the original findings. Fig. 1

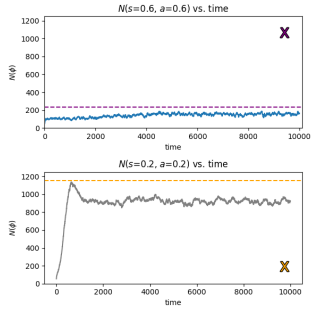

(a) Re-implemented population size $N(\phi)$ over time, with mean-field prediction of the steady-state size n^*.

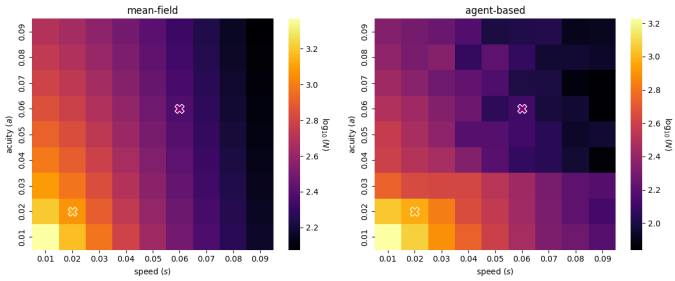

(b) Re-implemented mean-field prediction (left) and equilibrium population size from agent-based simulations (right).

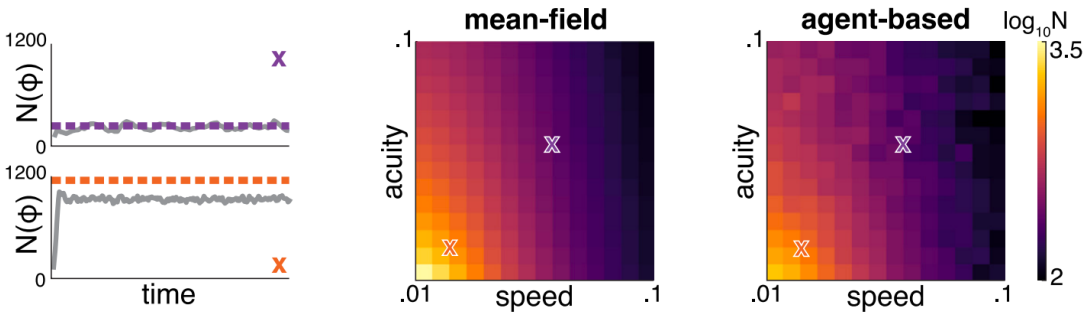

(c) Original results from [Kim et al. 2025] showing $N(\phi)$, the mean-field approximation n^*, and agent-based simulation outcomes.

Fig. 3. **Steady-state size of a homogeneous population.** Solid curves represent the population size $N(\phi)$; dashed lines indicate the mean-field approximation of the steady-state size n^*. Example phenotypes with high (top) and low (bottom) metabolism are marked with crosses. Top row: our reimplementation. Bottom row: original results from [Kim et al. 2025].

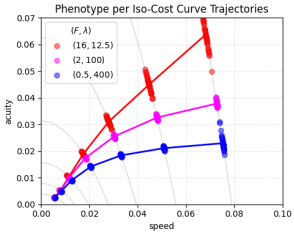

(a) Re-implemented results showing surviving phenotypes under iso-cost competition across environments.

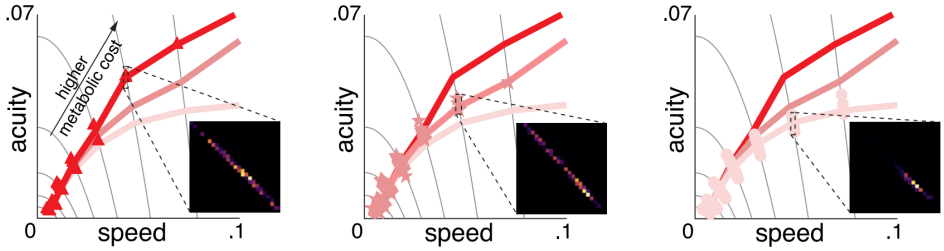

(b) Original results from [Kim et al. 2025] showing surviving phenotypes under iso-cost competition across environments.

Fig. 4. **Competition between foraging strategies with equal metabolic cost.** Each heavy curve connects the average surviving phenotypes at different metabolic costs. Colors and markers indicate resource environments.

shows net energy gain rate $\epsilon(s, a|r)$ exhibiting nearly identical trends across all tested resource densities, while Fig. 2 confirms that our reimplemented $L(a|r)$ curves closely match the original patterns. However, our derivative calculations $\frac{d}{da}[g^2(a|r)]$ display less smooth transitions and a narrower range compared to the original results. These minor quantitative differences are likely attributable to our discrete increment step choices ($\Delta s = \Delta a = 0.01$) creating more abrupt changes in the numerical differentiation process, and could potentially be resolved through finer parameter resolution.

Fig. 3 shows results consistent with expectations from the original study.

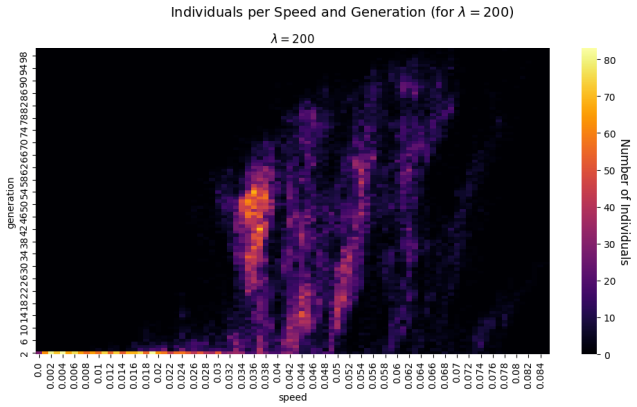

(a) Reimplementation results for the individual phenotypes at equilibrium across resource densities.

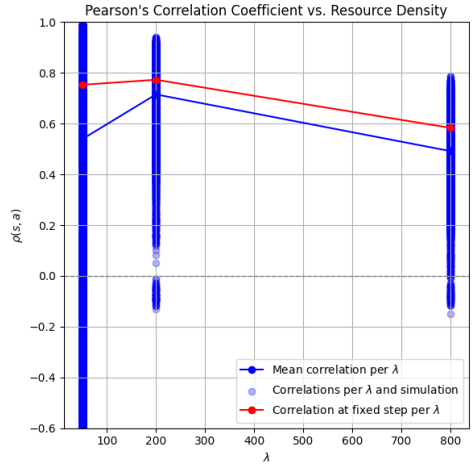

(b) Reimplementation results for the $\rho(s, a)$ as a function of resource density.

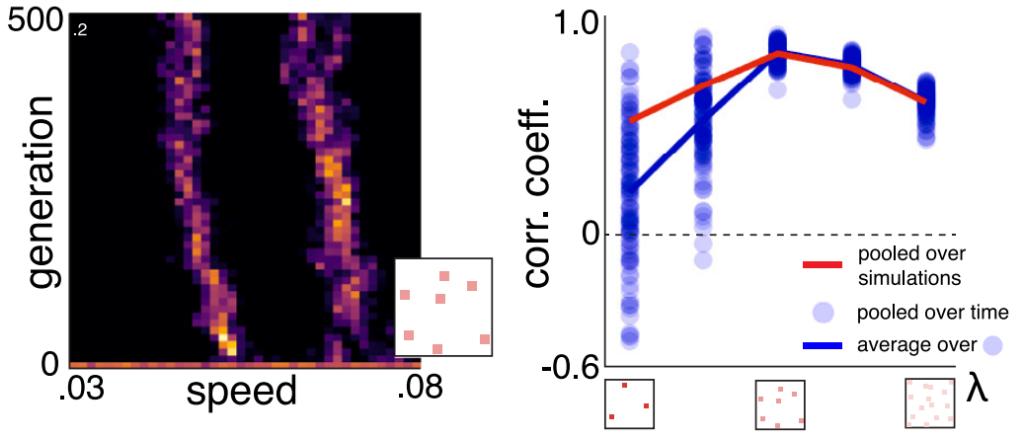

(c) Original results from [Kim et al. 2025] for the individual phenotypes at equilibrium and $\rho(s, a)$ as functions of resource density.

Fig. 5. **The equilibrium distribution of phenotypes depends on resource density.** Top: our reimplementation showing both the distribution of phenotypes and the resulting correlations across environments. Bottom: original results from [Kim et al. 2025] for comparison.

The analysis of the iso-cost curve (Fig. 4 shows that the results are in line with the original findings. This is because the surviving phenotype distributions are similar across different resource environments. However, our results show greater variability around the predicted trajectories than the smoother curves in [Kim et al. 2025]. This increased scatter is likely due to our reduced simulation parameters, which involved fewer runs and shorter generation times than the extensive computational approach of the original study.

Fig. 6, the biggest difference of the simulations compared to the original, was the maximum generation limit, which was a lot lower than the original paper and the reason for this was the high computational power required and time constrains. With that said, the results showed in Fig. 6 are very comparable, with similar pattern for individuals per speed and acuity. In Fig. 5b a) although the results clearly differ from the original paper, the conclusion that at intermediate resource density multiple distinct phenotypes coexist over many generations remains.

In the correlation graph, we got similar results to the original (even with only 3 environment parameters), with the biggest difference being the correlation over all simulation with $\lambda = 50$, but that could be explained by the fixed time step chosen.

While we successfully reproduce the general clustering patterns of the phenotypic analysis (Fig. 6) at low and high resource densities, we fail to observe the two distinct clusters reported by [Kim et al. 2025] in the intermediate resource density condition $\lambda = 300$. This discrepancy likely arises from our computational limitations

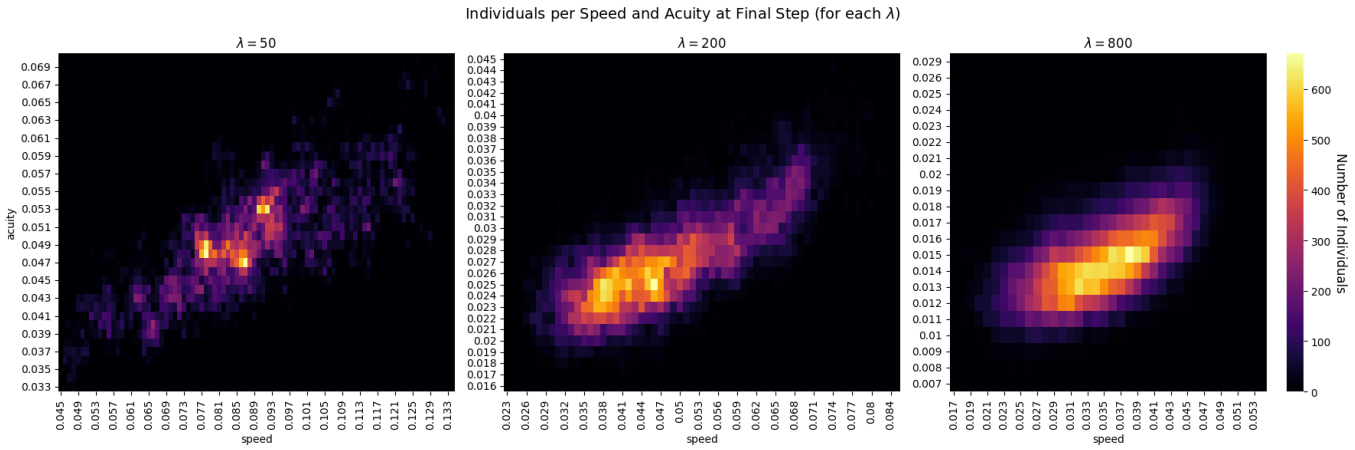

(a) Reimplementation of the phenotypic distributions ($\phi = (s, a)$) at equilibrium across resource densities.

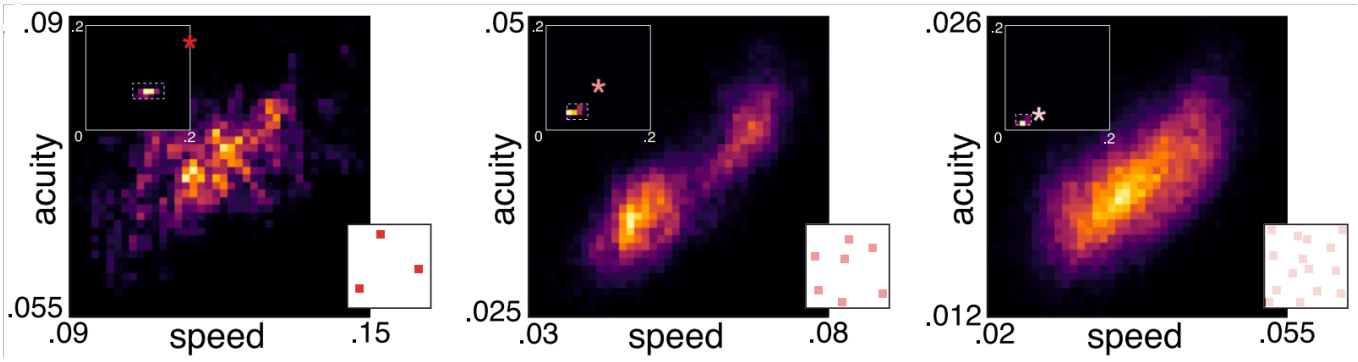

(b) Original results from [Kim et al. 2025] of the phenotypic diversity at equilibrium.

Fig. 6. **The equilibrium distribution of phenotypes depends on resource density.** Top: our reimplementation showing distinct clusters of phenotypes in intermediate environments. Bottom: original results from [Kim et al. 2025].

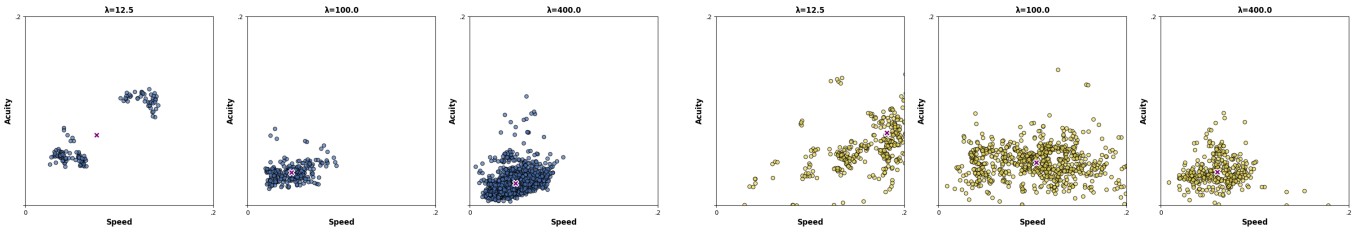

(a) Obtained scatterplots for base agent.

(b) Obtained scatterplots for sloth agent.

The raptor agent gains a selective advantage in sparse environments, where its speed gives it access to limited resources. However, in resource-rich scenarios, its low energy efficiency becomes a disadvantage, allowing the basic agent to dominate due to its more economical foraging. The sloth agent performs well in low-resource environments by adopting a high-speed, medium-acuity phenotype, due to it's ability to not consume movement energy while idle. As resource availability increases, selection favours slower, more efficient phenotypes. The turtle agent has a broader phenotypic dispersion, perhaps because producing more offspring at a time leads to more genetic variance. This however does not translate to a fitter species, as the turtle agent did not perform particularly well in any scenario.

5 Conclusion

This study successfully replicated the core components of [Kim et al. 2025] model while introducing a novel extension through multi-species dynamics, a dimension not explored in the original

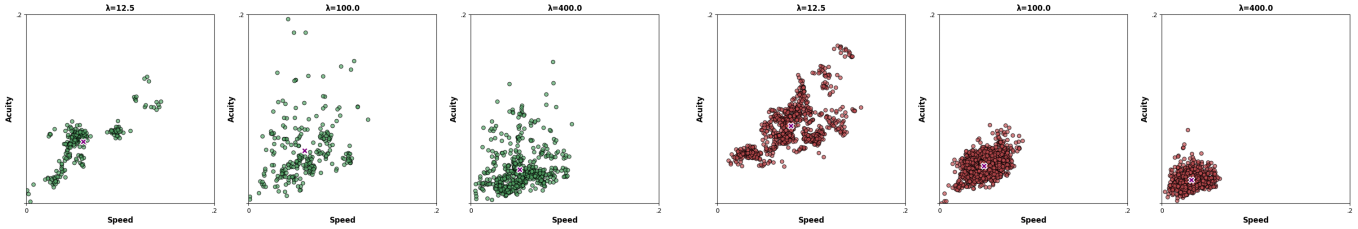

(a) Obtained scatterplots for turtle agent.

(b) Obtained scatterplots for raptor agent.

Fig. 8. Obtained phenotype scatterplots for the agent variations.

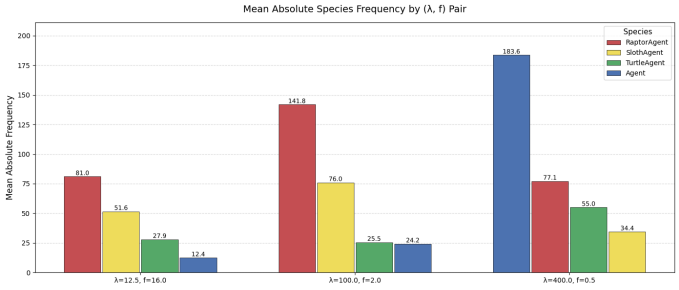

Fig. 9. Obtained mean absolute frequency of agents in last step by species for different λ

work. While our implementation does not perfectly reproduce every quantitative result from the original study, the overall patterns and qualitative behaviours align well with the published findings, demonstrating the robustness of the underlying theoretical framework.

The addition of multi-species interactions opens new avenues for understanding competitive dynamics in heterogeneous populations, suggesting that real-world ecological systems may display even richer behavioural patterns than previously recognised.

Future work could build upon our multi-species foundation to explore more complex environmental scenarios, investigate alternative evolutionary pressures, and bridge the gap between theoretical models and empirical ecological data.

References

Peter A. Abrams. 2000. The evolution of predator-prey interactions: theory and evidence. *Annual Review of Ecology and Systematics* 31 (2000), 79–105.

Eric L. Charnov. 1976. Optimal foraging, the marginal value theorem. *Theoretical Population Biology* 9, 2 (1976), 129–136.

Fiveable. 2024. 6.5 Foraging Strategies and Trade-offs – Animal Behavior. https://library.fiveable.me/animal-behavior/unit-6/foraging-strategies-trade-offs/study-guide/21a884oT67tAdnRV Accessed 8 June 2025.

Stephen Jay Gould. 1989. *Wonderful Life: The Burgess Shale and the Nature of History.* W.W. Norton & Company, New York.

Libbie Hyman Hyman. 1940. *The Invertebrates: Protozoa through Ctenophora.* McGraw-Hill, New York.

Taehyeok Kim, Amaury Lambert, and Massimo Vergassola. 2025. Emergence of multiple foraging strategies under competition. *Mathematical Biosciences* 360 (2025), 109377. doi:10.1016/j.mbs.2025.109377

Simon A. Levin. 1992. The problem of pattern and scale in ecology. *Ecology* 73, 6 (1992), 1943–1967.

Ronald M. Nowak. 1999. *Walker's Mammals of the World.* Johns Hopkins University Press, Baltimore.

Gary Rosenberg et al. 2007. Hydra and limnomedusae: contrasting foraging strategies. *Journal of Experimental Biology* 210 (2007), 1234–1242.

Thomas T. Struhsaker. 1997. Ecology of Colobus Monkeys. *International Journal of Primatology* 18, 1 (1997), 1–20.

June 2025

Table 2. Summary of encountered issues, attempted solutions, and observed outcomes during replication.

Problem Encountered	**Attempted Solution**	**Result**
Unclear whether experiments in Section 3.1 were run once or averaged over multiple runs	Assumed single run due to omission; Sections 3.2 and 3.3 specify 100 runs	Single run assumed for Section 3.1
Increment steps for speed and acuity, and value of F not specified in Section 3.1	Used fixed increment $\Delta s = \Delta a = 0.01$, set $F = 1$ by assumption	Enabled systematic exploration of trait space
Number of steps, runs, and initial population size not specified in Section 3.2	Assumed $N = 50,500$ agents; ran simulations for 1000 steps	Consistent results obtained across tested conditions
Increment steps for speed and acuity, and value of F not specified in Section 321	Used fixed increment $\Delta s = \Delta a = 0.01$, set $F = 1$ by assumption	Enabled systematic exploration of trait space
Phenotypes used for convergence graphs in Section 3.2 not explicitly defined; only described as low/high metabolism	Selected representative phenotypes matching these qualitative descriptions	Observed convergence trends qualitatively similar to original study
Discrepancy between number of agents reported in Section 3.3 (10^3) and appendix (10^4 phenotypes)	Followed main text and used 10^3 agents	Population dynamics aligned with main text results
In the original paper, 3.3 experiment is repeat 100 times, with parameters used, which involves a lot of computational power	Time it took to run for 40 simulations was around 19 hours.	Only manage to extract data from 40 simulations.
In the original paper, 3.4 experiment is repeat 100 times, until 20000 or 500 generations of agents depending on environment parameters, which involves a lot of computational power	Due to time restrictions and lack of computational power, we reduced the number of generations to 400, 100, 50, with the respective enviroment parameters.	Only manage to extract data from 80 simulations.
In Section 3.3 graph D, it appears that data used was extracted from simulations with 5 different environment parameters, although the paper only mentions running simulations with 3,	Followed main text, and used data from only the 3 simulations with parameters provided.	Correlation coefficient graph only was data from 3 environments instead of 5.
Unclear whether birth and death decisions are mutually exclusive per generation	Modeled birth and death as independent events potentially occurring in the same generation	Captured richer population dynamics